The Journal of Immunology

Resolvin D1 and Resolvin D2 Govern Local Inflammatory Tone in Obese Fat

Joan Clària, Jesmond Dalli, Stephanie Yacoubian, Fei Gao and Charles N. Serhan

J Immunol 2012; 189:2597-2605; Prepublished online 27 July 2012;
doi: 10.4049/jimmunol.1201272
http://www.jimmunol.org/content/189/5/2597

The Journal of Immunology is published twice each month by
The American Association of Immunologists, Inc.,
1451 Rockville Pike, Suite 650, Rockville, MD 20852

Print ISSN: 0022-1767 Online ISSN: 1550-6606.

Resolvin D1 and Resolvin D2 Govern Local Inflammatory Tone in Obese Fat

Joan Clària,[1] Jesmond Dalli, Stephanie Yacoubian, Fei Gao, and Charles N. Serhan

The unprecedented increase in the prevalence of obesity and obesity-related disorders is causally linked to a chronic state of low-grade inflammation in adipose tissue. Timely resolution of inflammation and return of this tissue to homeostasis are key to reducing obesity-induced metabolic dysfunctions. In this study, with inflamed adipose, we investigated the biosynthesis, conversion, and actions of Resolvins D1 (RvD1, 7*S*,8*R*,17*S*-trihydroxy-4*Z*,9*E*,11*E*,13*Z*,15*E*,19*Z*-docosahexaenoic acid) and D2 (RvD2, 7*S*,16*R*,17*S*-trihydroxy-4*Z*,8*E*,10*Z*,12*E*,14*E*,19*Z*-docosahexaenoic acid), potent anti-inflammatory and proresolving lipid mediators (LMs), and their ability to regulate monocyte interactions with adipocytes. Lipid mediator-metabololipidomics identified RvD1 and RvD2 from endogenous sources in human and mouse adipose tissues. We also identified proresolving receptors (i.e., ALX/FPR2, ChemR23, and GPR32) in these tissues. Compared with lean tissue, obese adipose showed a deficit of these endogenous anti-inflammatory signals. With inflamed obese adipose tissue, RvD1 and RvD2 each rescued impaired expression and secretion of adiponectin in a time- and concentration-dependent manner as well as decreasing proinflammatory adipokine production including leptin, TNF-α, IL-6, and IL-1β. RvD1 and RvD2 each reduced MCP-1 and leukotriene B_4-stimulated monocyte adhesion to adipocytes and their trans-adipose migration. Adipose tissue rapidly converted both resolvins (Rvs) to novel oxo-Rvs. RvD2 was enzymatically converted to 7-oxo-RvD2 as its major metabolic route that retained adipose-directed RvD2 actions. These results indicate, in adipose, D-series Rvs (RvD1 and RvD2) are potent proresolving mediators that counteract both local adipokine production and monocyte accumulation in obesity-induced adipose inflammation. ***The Journal of Immunology*****, 2012, 189: 2597–2605.**

Expansion of adipose tissue mass in obesity is causally linked to a chronic state of "low-grade" inflammation driven by infiltrated macrophages in this tissue (1–5). The presence of increased numbers of macrophages forming characteristic "crownlike structures" that surround necrotic adipocytes and scavenge adipocyte debris is a prevalent pathological trait in obesity (6). Although enlarged adipocytes were initially thought to be the cellular source of proinflammatory mediators in obesity, it was later established that the presence of infiltrated macrophages in inflamed fat perpetuates a vicious cycle of monocyte recruitment and exacerbates production of proinflammatory adipokines (4–6). This persistent state of inflammation, also known as "metabolic-triggered inflammation" or "metainflammation," in adipose tissue is deleterious, increasing the incidence of metabolic syndrome and obesity-related comorbidities including dyslipidemia, as well as several forms of cardiovascular disease (1–3). The key sequela of adipose tissue inflammation is insulin resistance leading to type 2 diabetes and nonalcoholic fatty liver disease (1–3).

Prolonged, unremitting inflammation in adipose tissue has a negative impact on insulin-sensitive tissues; hence, its timely resolution could be a critical step toward regaining metabolic balance. Resolvins (Rv) and protectins are the first proresolving mediators biosynthesized from essential n-3 fatty acids that stimulate active resolution of acute inflammation and return to homeostasis (7, 8). Unlike their precursors docosahexaenoic acid (DHA) and eicosapentaenoic acid (EPA), Rvs exert potent actions in the picomolar to nanomolar range, for example, counterregulating proinflammatory signaling pathways and acting as "braking signals" of the persistent vicious cycle leading to unremitting inflammation (for a review, see Ref. 8). These endogenous autacoids show remarkable potency resolving inflammation-related diseases in animal models of periodontitis, asthma, and colitis (8). Because increasing dietary ω-3 fatty acids reduces obesity-associated complications (9–11), the purpose of this study was to test the hypothesis that Resolvins D1 (RvD1, 7*S*,8*R*,17*S*-trihydroxy-4Z,9E,11E,13Z,15E,19Z-docosahexaenoic acid) and D2 (RvD2, 7*S*,16*R*,17*S*-trihydroxy-4Z,8E,10Z,12E,14E,19Z-docosahexaenoic acid) can attenuate adipose inflammation, and investigate their production and conversion by adipose tissues.

Materials and Methods

Mice

C57BL/6 mice with diet-induced obesity (60 kcal% high fat up to 16 wk) and control mice were from The Jackson Laboratory (Bar Harbor, ME). The

Center for Experimental Therapeutics and Reperfusion Injury, Department of Anesthesiology, Perioperative and Pain Medicine, Brigham and Women's Hospital and Harvard Medical School, Boston, MA 02115

[1]Current address: Department of Biochemistry and Molecular Genetics and Department of Physiological Sciences I, Hospital Clinic, University of Barcelona, Barcelona, Spain.

Received for publication May 4, 2012. Accepted for publication July 3, 2012.

This work was supported by the National Institutes of Health (Grants P01GM095467 and R01-GM038765 to C.N.S.), Spanish Health, Science and Innovation Ministries (Grants SAF09/08767 and BA10/00036 to J.C.), and the Spanish Association for the Study of Liver Diseases (Beca Hernández-Guío to J.C.).

Address correspondence and reprint requests to Prof. Charles N. Serhan, Center for Experimental Therapeutics and Reperfusion Injury, Department of Anesthesiology, Perioperative and Pain Medicine, Brigham and Women's Hospital, Harvard Institutes of Medicine, 77 Avenue Louis Pasteur, Boston, MA 02115. E-mail address: cnserhan@zeus.bwh.harvard.edu

The online version of this article contains supplemental material.

Abbreviations used in this article: DHA, docosahexaenoic acid; EOR, eicosanoid oxidoreductase; EPA, eicosapentaenoic acid; HETE, hydroxyeicosatetraenoic acid; LC-MS/MS, liquid chromatography tandem mass spectrometry; LM, lipid mediator; LTB_4, leukotriene B_4; LXA_4, lipoxin A_4; MRM, multiple reaction monitoring; PD1, protectin D1; 15-PGDH, 15-hydroxy/oxo-eicosanoid oxidoreductase; RP-HPLC, reverse-phase HPLC; Rv, resolvin; RvD1, Resolvin D1, 7*S*,8*R*,17*S*-trihydroxy-4*Z*,9*E*,11*E*,13*Z*,15*E*,19*Z*-docosahexaenoic acid; RvD2, Resolvin D2, 7*S*,16*R*,17*S*-trihydroxy-4*Z*,8*E*,10*Z*,12*E*,14*E*,19*Z*-docosahexaenoic acid; SPM, specialized proresolving mediator.

high-fat model is a reproducible model of obesity and pre-type 2 diabetes, and closely mirrors human obesity, most of which is thought to occur in response to high fat intake (12). For the C57BL/6J strain, average percentage weight gain is typically ~43% at the 16th week of feeding, and the variation among animals within the same diet group is <10%. Experiments were performed in accordance with the Harvard Medical School Standing Committee on Animals guidelines for animal care and approved protocol #02570.

Immunohistochemistry

Adipose tissue was fixed in 3.3% formalin, paraffin embedded, and sectioned at the Research Pathology Core of the Dana-Farber/Harvard Cancer Center (Boston, MA). Distribution of ALX/FPR2 receptor was detected using a rabbit anti-mouse ALX/FPR2 Ab (1/250; Santa Cruz Biotechnology, Santa Cruz, CA). Color was developed using Vectastain ABC Kit (Vector Laboratories, Burlingame, CA), and sections were counterstained with hematoxylin. Distribution of ChemR23 was detected using a rat anti-mouse ChemR23 Ab labeled with PE (eBioscience, San Diego, CA). Sections were visualized at magnification ×200 imaged with a Zeiss YFL microscope (Thornwood, NY) and ImagePro Plus 7 software (Media Cybernetics, Bethesda, MD).

Adipose tissue explants and ex vivo incubations

Epididymal fat pads from obese mice were collected under sterile conditions and placed in a P60 plate with prewarmed (37˚C) Dulbecco's phosphate-buffered saline containing penicillin (100 U/ml) and streptomycin (100 mg/ml). Connective tissue and blood vessels were removed by dissection before cutting the tissue into small pieces (<10 mg). Explants were cultured in DMEM with L-glutamine (2 mM), penicillin (50 U/ml), streptomycin (50 mg/ml), and 2% fatty acid-free BSA. Adipokine secretion and mRNA expression were assessed in explants incubated with vehicle (0.01% EtOH), rosiglitazone (0.3–10 μM), RvD1 (10 nM), RvD2 (10 nM), 17*R*-RvD1 (0.01–100 nM), lipoxin A_4 (LXA_4) (10 nM), or with equimolar concentrations (10 nM) of a mixture of RvD1, RvD2, 17*R*-RvD1, and LXA_4 for 4, 6, 12, and 24 h at 37˚C. To assess RvD1, RvD2, and 17*R*-RvD1 metabolism by adipose tissue, we initiated incubations by adding 1 μg of the selected compound at 37˚C for 0.5, 6, and 12 h. In some experiments, incubations were carried out in the presence of 100 μM indomethacin or α-methylcinnamic acid. Incubations were stopped with cold methanol (2 vol), and samples were taken to C18 solid phase extraction and subjected to liquid chromatography tandem mass spectrometry (LC-MS/MS).

Isolation and culture of adipocytes

Mouse fat pads were excised, rinsed two times in cold carbogen-gassed (5% CO_2:95% O_2) Krebs-Ringer, and minced into fine pieces. Minced samples were placed in Krebs-Ringer supplemented with 1% fatty acid-free BSA and 2 mM EDTA, and centrifuged at 500 × *g* for 5 min at 4˚C to remove free erythrocytes and leukocytes. Tissue suspensions (1 g) were placed in 5 ml Krebs-Ringer buffer supplemented with 1% fatty acid-free BSA and 1 mg/ml collagenase A, and incubated at 37˚C for 60 min with gentle shaking. Tissue homogenates were filtered through a 100-μm nylon mesh and then centrifuged at 500 × *g* for 5 min. Floating cells were collected, washed two times in carbogen-gassed DMEM supplemented with L-glutamine (2 mM), penicillin (100 U/ml), streptomycin (100 mg/ml), and HEPES (100 mM), and suspended in this DMEM medium containing 0.2% endotoxin-free fatty acid-free BSA before counting and plating on 12- or 96-well plates.

Lipid mediator-metabololipidomics

LC-MS/MS–based metabololipidomics was performed using linear ion trap triple quadrupole mass spectrometer (3200 QTRAP; Applied Biosystems, Foster City, CA) equipped with two HPLC pumps (LC-20AD; Shimadzu, Kyoto, Japan) coupled to an Eclipse Plus C18 reverse-phase column (4.6 mm × 50 mm × 1.8 μm; Agilent Technologies, Palo Alto, CA). The mobile phase consisted of MeOH/H_2O/acetic acid at a ratio of 60:40:0.01 (v/v/v) and ramped to 80:20:0.01 after 10 min and to 100:0:0.01 after 12 min. Instrument control and data acquisition were performed using Analyst 1.5 software (Applied Biosystems). Ion pairs from reported multiple reaction monitoring (MRM) methods (13) were used for profiling and quantification of bioactive lipid mediators (LMs). Quantification was performed using standard calibration curves for each, and recoveries were calculated using deuterated internal standards (d4-leukotriene B_4 [d4-LTB_4], d4-PGE_2, and d8-5-hydroxyeicosatetraenoic acid [d8-5-HETE]) purchased from Cayman Chemical (Ann Arbor, MI).

Enzymatic conversion

RvD1, RvD2, and 17*R*-RvD1 (100 ng) were taken to dryness under N_2 stream and incubated with recombinant human 15-PG-dehydrogenase/eicosanoid oxidoreductase (EOR; 0.5 U; Cayman Chemical) in 100 μl Tris-HCl buffer (50 mM, pH 7.4) containing NAD^+ (1.0 mM). EOR activity was monitored spectrophotometrically by the formation of NADH from NAD^+ at 340 nm. Enzymatic conversion of RvD1, RvD2, and 17*R*-RvD1 (100 ng) was also tested in 100-μl incubations of Tris-HCl buffer (50 mM, pH 7.4) containing NADPH (0.1–0.5 mM) and 11β-hydroxysteroid dehydrogenase type 1 (2 U; Cayman Chemical). All incubations were allowed to proceed for 30 min at 37˚C and stopped with cold methanol before C18 solid-phase extraction for further analyses using LC-MS/MS.

Oxo-RvD2 products

RvD2 (1.5 mg) in ethanol was dried down under N_2 stream and suspended in buffer containing Tris-HCl (100 μl, 50 mM, pH 7.4) and NAD^+ (1.0 mM). Enzymatic conversion was initiated by the addition of recombinant human EOR (0.5 U) and allowed to proceed for 30 min at 37˚C. After 30 min, reactions were stopped with cold methanol and taken for C18 solid-phase extraction. Oxo-containing products were isolated in a Hewlett-Packard 1100 Series HPLC system equipped with a Phenomenex Luna C18 (150 mm × 2 mm × 5 μm) column and a diode array detector. Products were eluted with MeOH/H_2O/acetic acid (70:30:0.01) as phase one (*t*0, −10 min) and a linear gradient with MeOH/acetic acid (99.9:0.1) as phase two (10–30 min), at a flow rate of 0.2 ml/min.

Adipokines and cytokines

Adiponectin and leptin levels in supernatants from adipose tissue explants were quantified by enzyme immunoassay (Cayman Chemical). Concentrations of TNF-α, IL-6, IL-12, IL-10, IL-1β, IL-13, IL-33, and IL-4 were assessed by a custom-made Luminex multiplex cytokine-detection bead assay platform using a Luminex 200 instrument (Luminex, Austin, TX). The assay was conducted using 20 μl of supernatants from adipose tissue explants. Data acquisition and analysis were conducted using StarStation software v2.3 (Applied Cytometry Systems, Dinnington, U.K.).

RNA isolation, reverse transcription, and real-time PCR

Total RNA from adipose tissue was isolated using the TRIzol reagent. RNA concentration was assessed in a NanoDrop-1000 spectrophotometer (NanoDrop Technologies, Wilmington, DE). cDNA synthesis from 100–200 ng total RNA was performed using the Omniscript kit (Qiagen, Hilden, Germany). Real-time PCR was performed with validated and predesigned QuantiTect Primer Assays (Qiagen) for adiponectin (QT01048047) and EOR (QT01039192) or TaqMan Gene Expression Assays for MCP-1 (Mm00441242_m1) using GAPDH (QT01192646) as endogenous control. Real-time PCR amplifications were carried out in an ABI 7900HT thermal cycler (Applied Biosystems). Relative quantification of gene expression was performed using the comparative C_t method. Conventional PCR amplification of mouse ChemR23 and ALX/FPR2 and human ChemR23, ALX/FPR2, GPR32, and GAPDH was performed with specific primer pairs. PCR products were analyzed by electrophoresis in 2.0% agarose gels and visualized by ethidium bromide staining.

Monocyte–adipocyte assays

Murine bone marrow-derived monocytes were isolated using the EasySep mouse monocyte-enrichment kit (StemCell Technologies, Vancouver, BC, Canada). After isolation, cells were counted and resuspended in PBS^{2+} containing 0.1% BSA at a density of 2×10^6 cells/ml. Mouse adipocytes were isolated as described earlier and resuspended in DMEM at 0.9×10^6 cells/ml, and 25,000 cells/well were loaded onto a 96-well ChemoTx plate (Neuro Probe, Gaithersburg, MD) with polycarbonate membrane filters and 3-μm membrane pores, which require modest amounts of testing compounds. Adipocytes were incubated for 1 h at 37˚C, subsequently either LTB_4 (10 nM) or MCP-1 (15 ng/ml) was added to the lower wells, and the isolated monocytes were then loaded on top of membrane in the presence of 10 nM RvD1, RvD2, 17*R*-RvD1, 17(*R/S*)-methyl-RvD1 (from Dr. Nicos Petasis, University of Southern California, and prepared as in Kasuga et al. [14]), or the corresponding RvD1 and RvD2 oxo-containing products. Cells were then coincubated for 90 min at 37˚C. The cells that did not transmigrate were washed, whereas the transmigrated cells along with adipocytes were immunofluorescent stained as detailed later. The number of transmigrated monocytes and the number of monocytes adhered to adipocytes were assessed by using a rabbit anti-perilipin polyclonal Ab (1 μg/ml; Abcam, Cambridge, MA) in combination with a donkey anti-

rabbit PE-conjugated Ab and a rat anti-mouse CD11b or a mouse anti-human CD11b FITC-conjugated Ab (eBioscience). Staining was assessed on a FACSCanto II flow cytometer using BD FACSDiva 4.1 software (Becton Dickinson, San Jose, CA). The number of transmigrated monocytes was calculated as a function of the number of $CD11b^+$, $perilipin^-$ cells. Monocyte–adipocyte interactions were quantified by measuring CD11b levels in the $perilipin^+$ cells. In a separate set of experiments, the chemotactic properties of RvD1, RvD2, and the oxo-containing RvD1 and RvD2 metabolites were assessed by loading the compounds in the bottom well of the ChemoTx plates and loading the monocytes on top of the filter. Cells were then incubated for 90 min at 37°C, and the number of transmigrated cells was assessed as described earlier.

Human PBMC were isolated from healthy volunteer peripheral blood according to protocol #1999P001297 approved by the Partners Human Research Committee. In brief, blood collected in heparin was centrifuged ($200 \times g$) for 15 min removing the platelet-rich plasma fraction. Cells were then layered over Ficoll-Hypaque (Organon Teknika, Durham, NC) and centrifuged ($500 \times g$) for 35 min. The mononuclear cell layer was collected, washed once, and resuspended in PBS containing 2% FCS and 1 mM EDTA. PBMC were then isolated using a human monocyte isolation kit (StemCell Technologies) and resuspended in PBS^{2+} containing 0.1% BSA at a density of 2×10^6 cells/ml. Human s.c. fresh primary adipocytes (floaters) were obtained from obese individuals with a body mass index $\geq$ 30 and age between 39 and 46 y (Zenbio, Research Triangle Park, NC), and grown in DMEM at a concentration of 2×10^6 cells/ml. Monocyte transmigration to the stimulated human adipocytes (25,000 cells/well) was assessed as outlined earlier for the mouse cells. Monocyte–adipocyte interactions were assessed by measuring the CD11b expression levels in the $perilipin^+$ cells.

Results

First, we compared endogenous biosynthesis of proresolving mediators in adipose tissues from lean and obese mice. Adipose tissues were subjected to LC-MS/MS–based LM metabololipidomics (see *Materials and Methods*), and in profiles obtained from adipose tissue, we identified RvD1, RvD2, and protectin D1 (PD1: 10*R*,17*S*-dihydroxy-4*Z*,7*Z*,11*E*,13*E*,15*Z*,19*Z*-docosahexaenoic acid) from endogenous sources in both lean and obese mice. Representative chromatograms of selected MRM (m/z 375 > 215, m/z 375 > 233, m/z 359 > 153) and representative tandem mass spectra for RvD1, RvD2, and PD1 are shown in Fig.

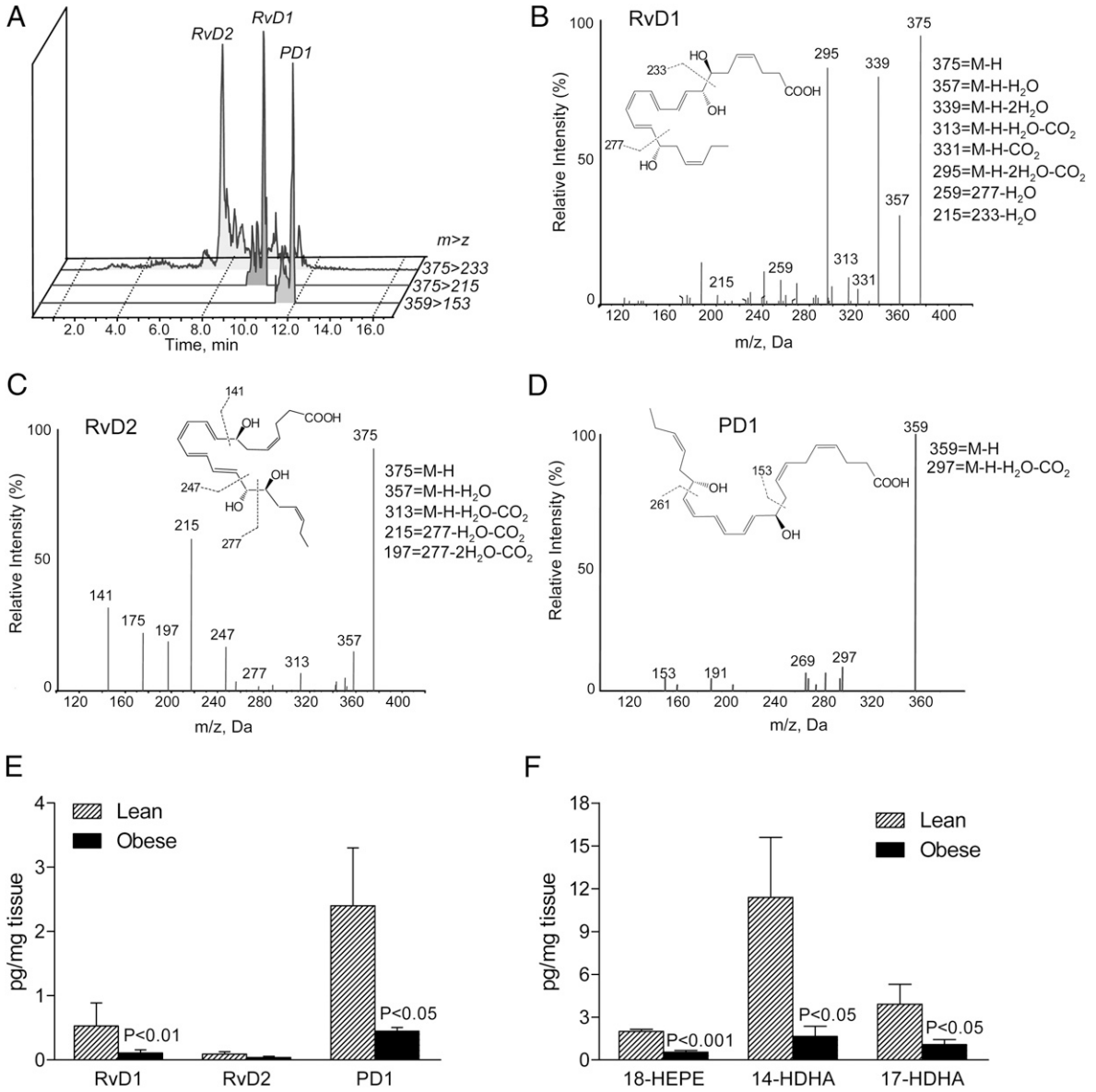

FIGURE 1. SPM in obese adipose tissue: LC-MS/MS–based LM-metabololipidomics. (**A**) MRM chromatograms (m/z 375 > 233, 375 > 215, and 359 > 153) and representative tandem mass spectra of RvD1 (**B**), RvD2 (**C**), and PD1 (**D**) in adipose tissue from obese mice. (**E**) Quantitation of SPM in adipose tissue from lean and obese mice. (**F**) Quantitation of monohydroxy markers of RvE1 and RvD1 biosynthetic pathways from EPA and DHA in adipose tissue from lean and obese mice. Results represent the mean ± SEM of five different individuals.

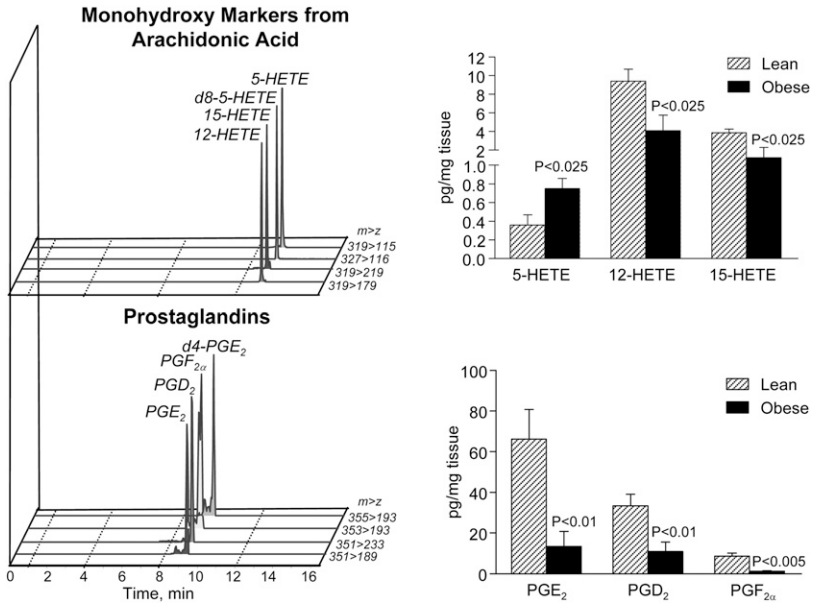

FIGURE 2. LC-MS/MS–based metabololipidomics of LMs derived from arachidonic acid in obese adipose tissue. Representative MRM chromatograms of monohydroxy markers from arachidonic acid and PGs (*left panels*), and their quantitation in adipose tissue from lean and obese mice (*right panels*). Results represent the mean ± SEM of five different individuals.

1A–D. Compared with lean animals, adipose tissue from obese mice had reduced levels of both RvD1 and PD1 (Fig. 1E). Also, levels of 17*S*-hydroxydocosahexaenoic acid (17*S*-hydroxy-4Z,7Z,10Z,13Z,15E,19Z-docosahexaenoic acid) and 18-hydroxyeicosapentaenoic acid (18*R*-hydroxy-5Z,8Z,11Z,14Z,16E-eicosapentaenoic acid), the monohydroxy markers of D-series and E-series Rv biosynthesis, were significantly lower in fat from obese mice (Fig. 1F). We also identified 14*S*-hydroxydocosahexaenoic acid (14*S*-hydroxy-4Z,7Z,10Z,12E,16Z,19Z-docosahexaenoic acid), a marker of maresin biosynthesis pathway including MaR1 (15) in these fat samples from obese mice that was also decreased (Fig. 1F).

Significant levels of eicosanoids derived from arachidonic acid, including 5-HETE, 12-HETE, 15-HETE, PGE_2, PGD_2, and $PGF_{2\alpha}$, were also present in these tissues (Fig. 2). Compared with lean adipose, obese adipose gave increased 5-HETE with reduced PG as well as 12-HETE and 15-HETE levels (Fig. 2).

Human adipocytes from obese patients were obtained and LM-metabololipidomics carried out to translate these findings. As shown in Fig. 3, the profiles of LM identified in human adipocytes were similar to those obtained from mouse adipocytes. However, mouse adipocytes produced higher amounts of RvD1, PD1, 14*S*-hydroxydocosahexaenoic acid, 17*S*-hydroxydocosahexaenoic acid, and 18-hydroxyeicosapentaenoic acid, as well as 12-HETE and 15-HETE, than human adipose (Fig. 3). Conversely, human adipocytes produced higher PGE_2, PGD_2, and $PGF_{2\alpha}$ than mouse adipocytes (Fig. 3), whereas the 5-lipoxygenase products 5-HETE, LTB_4, and LXA_4 were essentially similar in both species (Fig. 3).

Do adipose tissues express receptors for specialized proresolving mediators (SPM)? To address this, we assessed adipose tissue from lean and obese mice for expression of ALX/FPR2 and ChemR23 receptors for RvD1 and RvE1, respectively (16). Representative PCR analysis of mRNA receptor expression and immunohistochemistry are presented in Fig. 4A. In human cells, RvD1 also

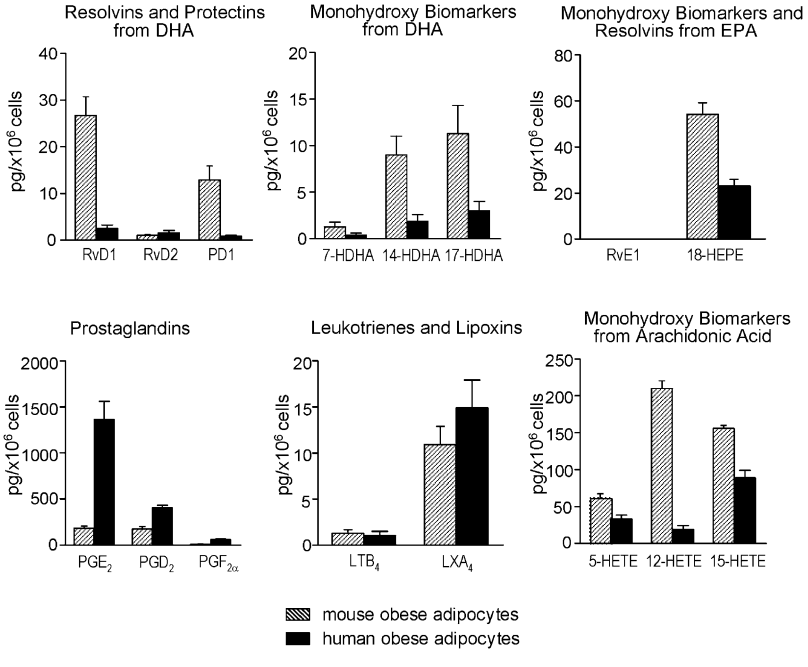

FIGURE 3. SPM and eicosanoids in human and mouse adipocytes: LC-MS/MS–based LM-metabololipidomics. Quantitation of indicated LMs in adipocytes isolated from epididymal fat pads of obese mice (shadowed bars) and adipocytes isolated from obese human s.c. fat samples (solid bars). Each compound was expressed as the quantity in picograms (pg) relative to 1×10^6 cells. Results are the mean ± SEM of three different individuals.

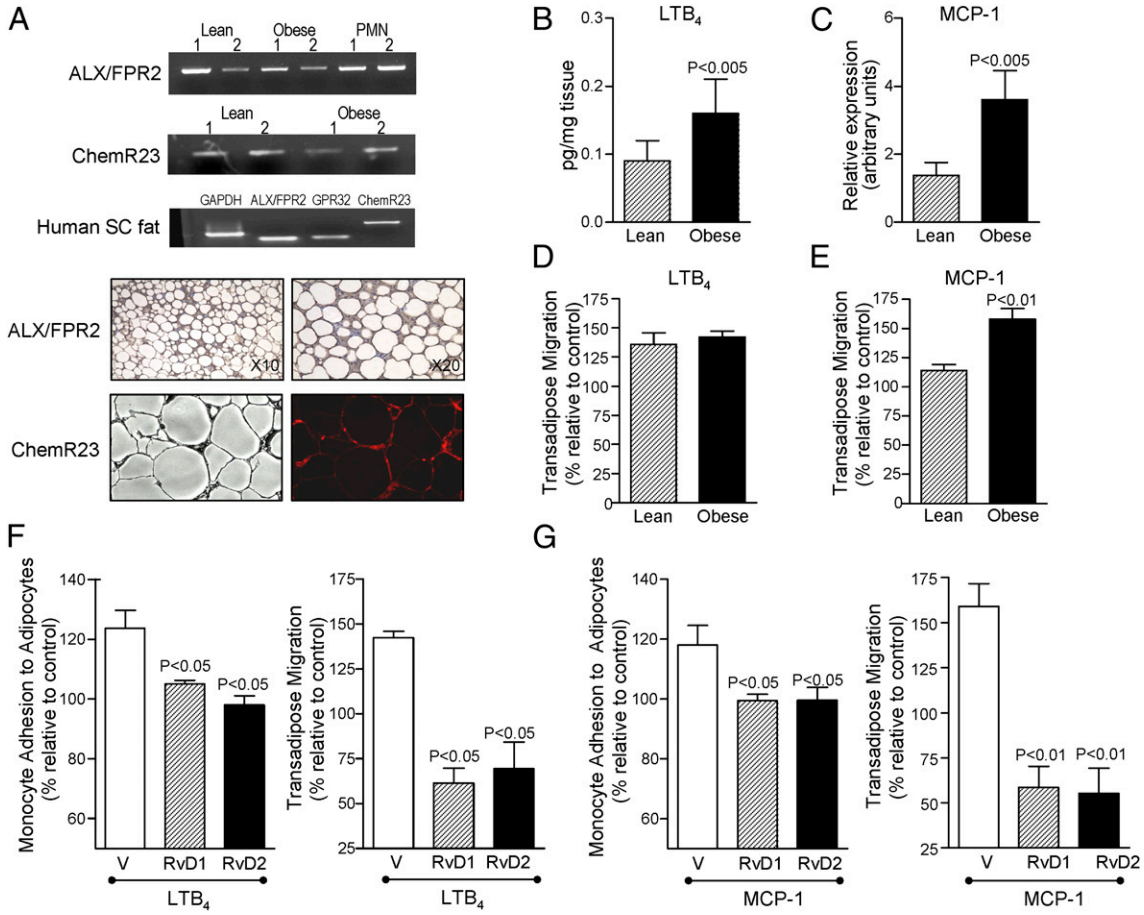

FIGURE 4. Proresolving mediator GPC receptors in adipose tissue, and RvD1 and RvD2 attenuation of monocyte adhesion to adipocytes and transadipose migration. (**A**) Representative PCR analysis of ALX/FPR2 and ChemR23 receptors in adipose tissue from lean and obese mice (*upper panels*); representative expression of ALX/FPR2, GPR32, and ChemR23 (original magnification ×40) receptors in human s.c. fat (*middle panel*); and representative photomicrographs of ALX/FPR2 and ChemR23 distribution in adipose tissue sections stained with either a primary rabbit anti-mouse ALX/FPR2 Ab or a rat anti-mouse ChemR23 Ab labeled with PE (*lower panels*). RNA from mouse PMN was used as positive control for ALX/FPR2 expression. (**B**) LTB_4 levels in adipose tissue from lean and obese mice. (**C**) MCP-1 mRNA expression in adipose tissue from lean and obese mice. (**D** and **E**) Transadipose migration of monocytes from lean and obese mice in response to LTB_4 (10 nM) (D) and MCP-1 (15 ng/ml) (E). Murine adipocytes were loaded onto a 96-well ChemoTx plate, and LTB_4 or MCP-1 was added in the lower wells. Monocytes were placed on top of 3-μm-pore filters and coincubated (90 min, 37°C). The number of transmigrated monocytes was assessed by flow cytometry using anti-CD11b Abs. (**F** and **G**) RvD1 and RvD2 actions on obese monocyte interactions with adipocytes. Murine adipocytes were loaded onto a 96-well ChemoTx plate, and LTB_4 (10 nM) (F) or MCP-1 (15 ng/ml) (G) was added in the lower wells. Monocytes were placed on top in the presence of 10 nM RvD1 or RvD2 and coincubated (90 min at 37°C; see *Materials and Methods*). Results are the mean ± SEM of three experiments in triplicate.

signals via GPR32 (16), which apparently is not present in murine cells, a receptor that was found to be constitutively expressed in human s.c. fat in addition to ALX/FPR2 and ChemR23 receptors (Fig. 4A). Hence, adipose tissue expresses the three presently known G protein-coupled receptors for RvD1, RvE1, and LXA_4.

To determine the functional relevance of RvD1 and RvD2 in inflamed adipose, we assessed their impact on adhesion of monocytes to adipocytes and monocyte transadipose migration, which are critical events in mounting a strong inflammatory response within obese adipose (4, 5). To this end, we used established cellular responses in a 96-well ChemoTx plate. These were performed by adding a chemotactic stimulus, either MCP-1 or LTB_4, to the bottom wells, with 25,000 adipocytes suspended below the membrane and 50,000 monocytes placed above the membrane in the presence of either RvD1 or RvD2. MCP-1 and LTB_4 were used as monocyte chemoattractants because they were also increased in obese adipose tissue (Fig. 4B, 4C). Of interest, the chemotactic responses to MCP-1 (15 ng/ml) were significantly higher in monocytes obtained from obese mice compared with those from lean mice (Fig. 4E). Here, similar responses to LTB_4 (10 nM) were obtained (Fig. 4D).

Addition of LTB_4 to the bottom wells caused increased monocyte attachment to adipocytes and transadipose migration that were markedly reduced by 10 nM of either RvD1 or RvD2 (Fig. 4F). Similar inhibitory actions for RvD1 and RvD2 were obtained after addition of MCP-1 (Fig. 4G). No synergic actions were observed after simultaneous addition of equimolar RvD1 and RvD2 ($n = 3$). For purposes of direct comparison, RvD1 actions were compared with those obtained with 17*R*-RvD1 and its analog 17(*R/S*)-methyl-RvD1 (14), which resists rapid inactivation (Supplemental Fig. 1). Of interest, the inhibitory actions of RvD1 at nanomolar concentrations with monocyte chemotaxis were superior in monocytes from lean mice compared with those from obese mice (Supplemental Fig. 1). This suggests that obesity may activate circulating monocytes. Human adipocytes from obese patients were obtained and assessed as described earlier to translate these findings. With human adipocytes and monocytes, we found that the inhibitory actions of RvD1, RvD2, and 17*R*-RvD1 (10 nM each) on MCP-1 and LTB_4-induced monocyte adhesion to adipocytes and transadipose migration were similar to those observed with mouse cells (Supplemental Fig. 2A, 2B).

Adipose tissue inflammation and increased monocyte recruitment in obesity is accompanied by a dysregulated secretion of the antidiabetic and anti-inflammatory adipokine adiponectin, which is an essential homeostatic factor for systemic energy metabolism and insulin sensitivity (2). Consistent with this, mRNA expression and protein levels of adiponectin were consistently reduced in adipose tissues from obese mice (Fig. 5A). To explore whether SPM could rescue impaired adiponectin secretion in obesity, we exposed adipose tissue explants from obese mice to 10 nM RvD1, RvD2, LXA_4, or 17*R*-RvD1, as well as a mixture of SPM (as might be encountered in vivo), and adiponectin levels were monitored (at 12 h, 37˚C). Each SPM, including RvD1, RvD2, LXA_4, and 17*R*-RvD1, significantly increased adiponectin secretion (Fig. 5B). In this regard, the SPM mixture was the most potent.

Of note, the levels of leptin in supernatants of adipose tissue explants gradually declined with treatment, reaching statistical significance with RvD2 alone and with the SPM mixture (Fig. 5B). Next, we carried out concentration– and time–response experiments with 17*R*-RvD1, the SPM with the most potent actions on adiponectin. Incubation of adipose tissue explants with 17*R*-RvD1 increased adiponectin secretion in a concentration-dependent manner (Fig. 5C). This concentration–response curve proved to be bell-shaped like other bioactive LMs (17). Interestingly, 17*R*-RvD1 induced adiponectin to a similar extent to rosiglitazone, a known inducer of adiponectin production (18). However, the concentrations required for this thiazolidinedione were 1000 times higher than those required for 17*R*-RvD1 (Fig. 5C). Adiponectin gene regulation was assessed after 6 h of adipose tissue, revealing that RvD1, 17*R*-RvD1, and RvD2 significantly induced gene expression to levels similar to those observed after rosiglitazone treatment that was 300 times the concentration of Rv (Fig. 5D). The Rv precursor DHA at 10 nM did not induce adiponectin gene expression (n = 3). At the protein level, upregulation of adiponectin secretion by 17*R*-RvD1 and rosiglitazone peaked after 12 h (Fig. 5D).

Another hallmark of obesity and insulin resistance is increased secretion of inflammatory cytokines, mainly IL-6 and TNF-α, by adipose (2). To further assess the impact of Rvs on adipose tissue, we monitored cytokines after incubating fat explants with RvD1, RvD2, and 17*R*-RvD1. RvD1 drastically reduced levels of TNF-α, the proinflammatory and insulin-resistant adipokine (2), as well as IL-12 and IL-1β, whereas enhancing secretion of IL-10, an anti-inflammatory cytokine (19) (Fig. 6). With RvD1, the levels of IL-6, IL-33, IL-13, and IL-4 remained unchanged (Fig. 6). RvD2 and 17*R*-RvD1 reduced TNF-α, IL-1β, and IL-12, as well as IL-6 levels (Fig. 6). Together, these findings indicate that D-series Rvs have a unique role in dampening inflammation in adipose tissues.

Because local tissue inactivation of Rvs is a limiting step in their bioactions (20), we next examined whether adipose metabolically convert Rvs. LC-MS/MS profiling indicated that incubation of adipose tissue explants with RvD1, RvD2, or 17*R*-RvD1 resulted in their rapid loss (Fig. 7A). Within 30 min there was ~70% loss of RvD1 (Fig. 7A). In contrast, RvD2 and 17*R*-RvD1 were more resistant to conversion with ~70% of each remaining (Fig. 7A). Because RvD1 is rapidly inactivated by 15-hydroxy/oxo-eicosanoid oxidoreductase (15-PGDH) and EORs (20, 21), we next sought evidence for 15-PG-dehydrogenase/EOR expression in adipose tissue. As shown in Fig. 7B, expression in adipose tissue uncovered a remarkable upregulation of this oxidoreductase in obese mice. Interestingly, RvD1, RvD2, and 17*R*-RvD1 appeared to offer positive feedback regulation and increased EOR expression in adipose tissue explants to a similar extent as rosiglitazone, an established EOR inducer (Fig. 7C).

Based on their constitutive expression and role in determining adipose tissue catabolic activities (22), we next assessed whether inhibition of either EOR or other dehydrogenases, that is, 11β-hydroxysteroid dehydrogenase (Table I), impacts adipose tissue conversion of Rvs. To this end, we incubated adipose explants with Rvs in the presence of indomethacin, which along with

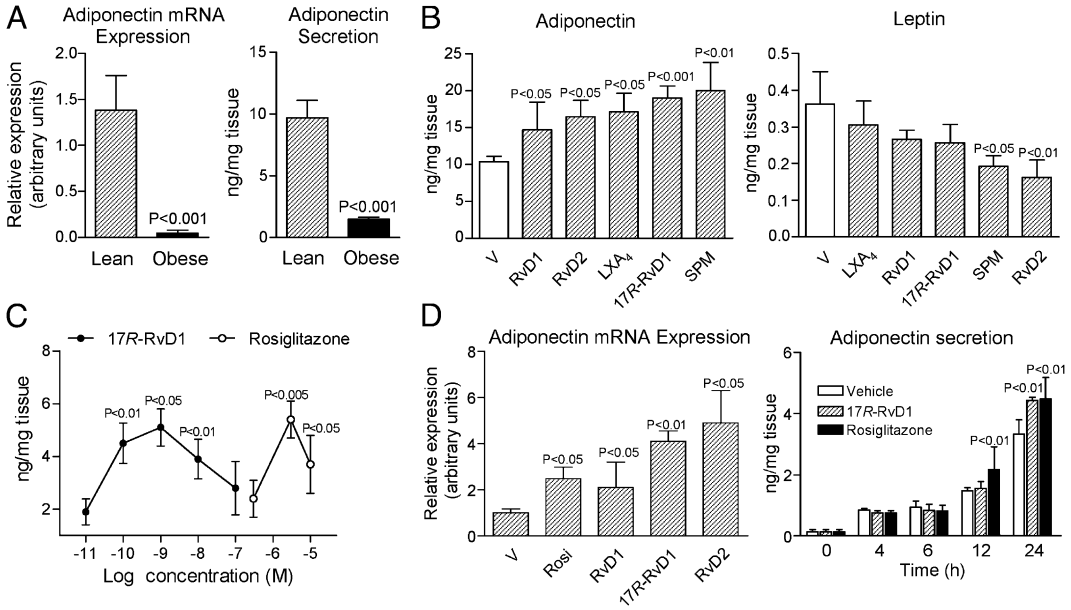

FIGURE 5. RvD1 and RvD2 potently induce adiponectin expression and secretion. (**A**) mRNA expression and tissue levels of adiponectin in fat from lean and obese mice. (**B**) Adipose tissue explants were incubated ex vivo with vehicle (0.01% EtOH) or 10 nM RvD1, RvD2, LXA_4, or 17*R*-RvD1 and a mixture of SPM (12 h at 37˚C). Adiponectin and leptin levels in supernatants were quantitated by enzyme immunoassay. (**C**) Concentration–response curves for 17*R*-RvD1 (0.01–100 nM) and rosiglitazone (0.3–10 μM) on adiponectin secretion. (**D**) Changes in adiponectin expression in adipose tissue after 6 h of treatment with rosiglitazone (rosi, 3 μM) and equiconcentrations (10 nM) of RvD1, 17*R*-RvD1, and RvD2 (*left panel*); and time–response for 17*R*-RvD1 (10 nM) and rosiglitazone (3 μM; *right panel*). Results are the mean ± SEM of five separate experiments.

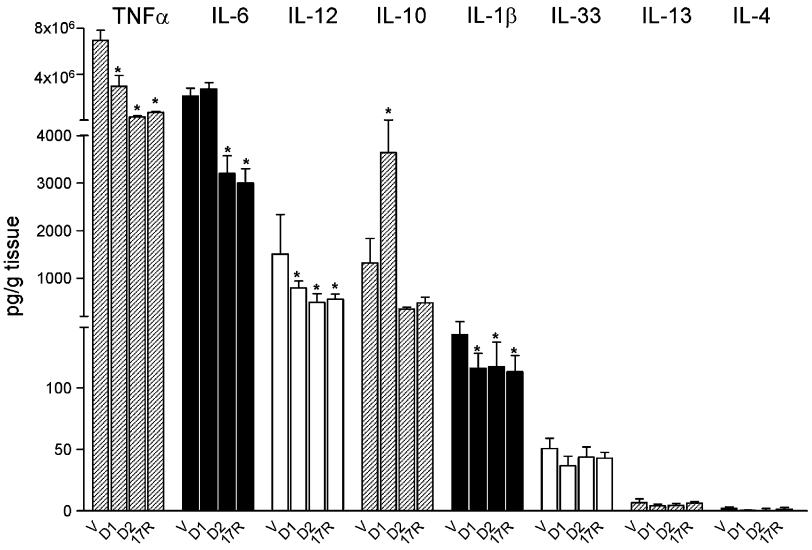

FIGURE 6. RvD1 and RvD2 regulate adipose tissue cytokine release. Cytokine measurements after addition of RvD1 (D1), RvD2 (D2), or 17*R*-RvD1 (17R; 10 nM, 12 h) were carried out using Luminex cytokine multiplex. Results represent the mean ± SEM of three experiments in duplicate. $*p < 0.05$ versus vehicle (V).

inhibiting COX is also a potent EOR inhibitor (21), or α-methylcinnamic acid, an 11β-hydroxysteroid dehydrogenase inhibitor (23). Addition of indomethacin resulted in ≥55% inhibition of RvD1 conversion, and α-methylcinnamic acid gave ~35% inhibition (Fig. 7D). These findings are also consistent with the notion that RvD1 is a substrate for both oxidoreductases. Indomethacin also blocked conversion of both RvD2 and 17*R*-RvD1 by ~30 and ~15%, respectively (Fig. 7D).

Because 15-PG-dehydrogenase/EOR oxidizes alcohols to their respective ketones (oxo) as in the conversion of PGE_2 (24), we determined the structure of these RvD1 and RvD2 further metabolites. RvD1 is further converted to both 8-oxo-RvD1 and 17-oxo-RvD1 (20), whereas the potential single oxo-containing product from RvD2 was expected to be either 7-oxo-RvD2 or 16-oxo-RvD2 (Fig. 8A, 8B). Hence, we assessed conversion of RvD2 by EOR, and using reverse-phase HPLC (RP-HPLC), we separated RvD2 and its further metabolites using their distinct chromatographic behavior and UV absorbance properties. RvD2 eluted from the RP-HPLC system at 19.3 min and the presence of a conjugated tetraene within RvD2 gave its characteristic triplet chromophore λ_{max}^{MeOH} 301 nm (Fig. 8C). The main metabolite derived from RvD2 conversion by recombinant human EOR eluted at 24.5 min and contained a single broad UV absorbance peak at λ_{max}^{MeOH} = 351 nm (Fig. 8C). This predominant further metabolic product of RvD2 was identified as 7-oxo-RvD2 using LC-MS/MS– and GC-MS–based analyses, and it was established as the initial oxidation product of RvD2 in obese adipose tissue (F.G., J.C., J.D., Sungwhan F. Oh, and C.N.S., manuscript in preparation). These results indicate that adipose tissue rapidly converts RvD2 by dehydrogenation to 7-oxo-RvD2, and emphasize that RvD2 further metabolism is governed by 15-PGDH, a process that is common in the local conversion and inactivation of other LMs including PGs, leukotrienes, and LXA_4 (24).

Next, each of the further metabolites of RvD1 and RvD2 were taken for direct comparisons of their bioactivity with that of the parent molecule. As shown in Fig. 8D and 8E, 8-oxo-RvD1 limited

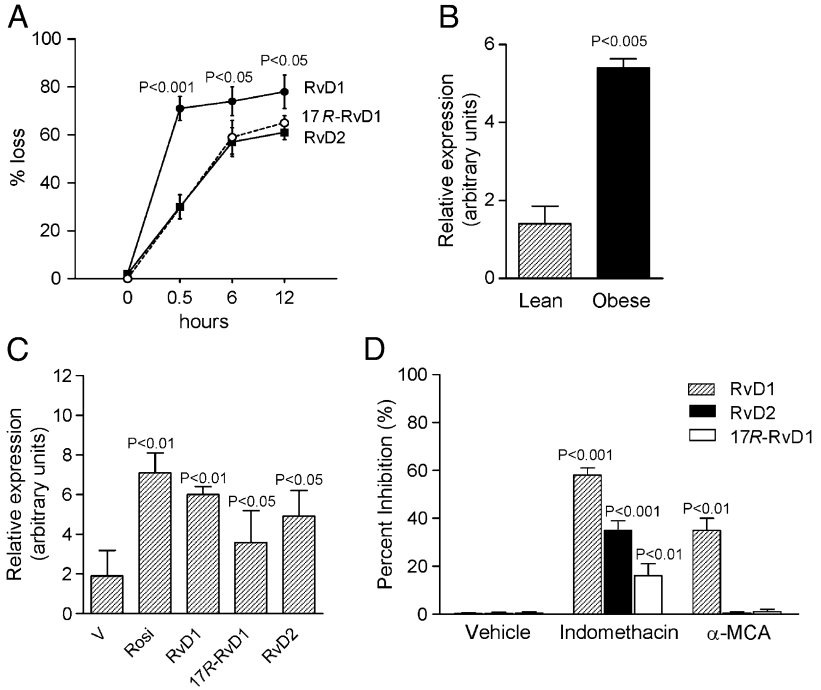

FIGURE 7. Rapid adipose tissue conversion of RvD1 and RvD2. (**A**) Time course of conversion by adipose tissue. RvD1, 17*R*-RvD1, and RvD2 were each added to fat explants, and incubations (37°C) were stopped with cold methanol (2 vol) at the indicated time intervals, extracted, and taken for LC-MS/MS. (**B**) mRNA expression for EOR in adipose tissue from lean and obese mice. (**C**) Upregulation of EOR in response to rosiglitazone (rosi, 3 μM), RvD1, RvD2, and 17*R*-RvD1 (10 nM each) treatment. (**D**) Inhibition of adipose tissue conversion of RvD1, RvD2, or 17*R*-RvD1 by indomethacin (indo, EOR inhibitor, 100 μM) and α-methylcinnamic acid (α-MCA, 11β-hydroxysteroid dehydrogenase type 1 inhibitor, 100 μM). RvD1, RvD2, and 17*R*-RvD1 were added to fat explants in the absence or presence of inhibitors, and 12 h later, incubations were stopped and extracted. Results are the mean ± SEM of four separate experiments.

Table I. RvD1, RvD2, and 17R-RvD1 conversion by oxidoreductases

	% Conversion		
	RvD1	RvD2	17*R*-RvD1
15-PG-dehydrogenase/EOR	68 ± 10	48 ± 5	20 ± 8
11β-Hydroxysteroid dehydrogenase	18 ± 3	0 ± 0	0 ± 0

RvD1, RvD2, or 17*R*-RvD1 (100 ng) were each incubated with recombinant human EOR (0.5 U) or recombinant human 11β-hydroxysteroid dehydrogenase type 1 (2.5 U) for 30 min at 37˚C. Reactions were stopped with 2 vol cold methanol, and solid phase extracted and taken for LC-MS/MS (see *Materials and Methods*).

MCP-1–induced monocyte adhesion to adipocytes and transadipose migration, whereas 17-oxo-RvD1 did not reduce monocyte recruitment in a statistically significant manner. These are consistent with those for PMN infiltration in vivo in murine peritonitis (20). Importantly, the new 7-oxo-RvD2, the predominant further metabolic product of RvD2 in adipose tissue, was essentially as active as RvD2 (~90% the activity of RvD2; Fig. 8F, 8G). In sharp contrast, 16-oxo-RvD2 was inactive. Of note, unlike MCP-1, monocytes showed no chemotactic response to RvD1, 8-oxo-RvD1, RvD2, or 7-oxo-RvD2 when these were added alone to the bottom wells for 90 min (Supplemental Fig. 2C).

Discussion

Results of these studies provide evidence of a heightened proinflammatory phenotype along with a compromised capacity to produce local SPM in obese adipose tissue. The mechanism(s) by which obesity results in a chronic proinflammatory phenotype within the adipose tissues are incomplete. In this context, hypoxia is a key driven force of chronic inflammation. Indeed, in the setting of obesity, an imbalance between the supply of and demand for oxygen in enlarged adipocytes causes tissue hypoxia and an increase in inflammatory adipokines (25). The resultant infiltration by macrophages and chronic low-grade inflammation promote, in turn, insulin resistance in adipose tissue (26).

In addition, the local tissue loss of proresolving mechanisms and mediators in inflammation such as SPM is critical and can contribute to obesity-linked inflammation and insulin resistance. Likely, this results from the lack of intrinsic capacity of adipose to generate appropriate endogenous "stop signals" and proresolving mediators for catabasis and the return to complete resolution (7, 27). A deficit in SPM in obese adipose tissue can be the consequence of the structural deficiency in the tissue content of ω-3 fatty acids, namely, DHA and EPA, as substrates for SPM biosynthesis (28). Because our findings also provide evidence that 15-PG-dehydrogenase/eicosanoid oxidoreductase, a key enzyme in SPM further metabolic conversion, is markedly upregulated in obese adipose tissue, the local loss of SPM in obesity may reflect accelerated tissue SPM conversion to inactive metabolites. Interestingly, this SPM deficiency in obesity appears to be a generalized defect in all metabolic tissues, because in addition to adipose, it is also present in liver and skeletal muscle (28). Taken together, these findings are consistent with the notion that unresolved, unremitting, chronic, "low-grade"

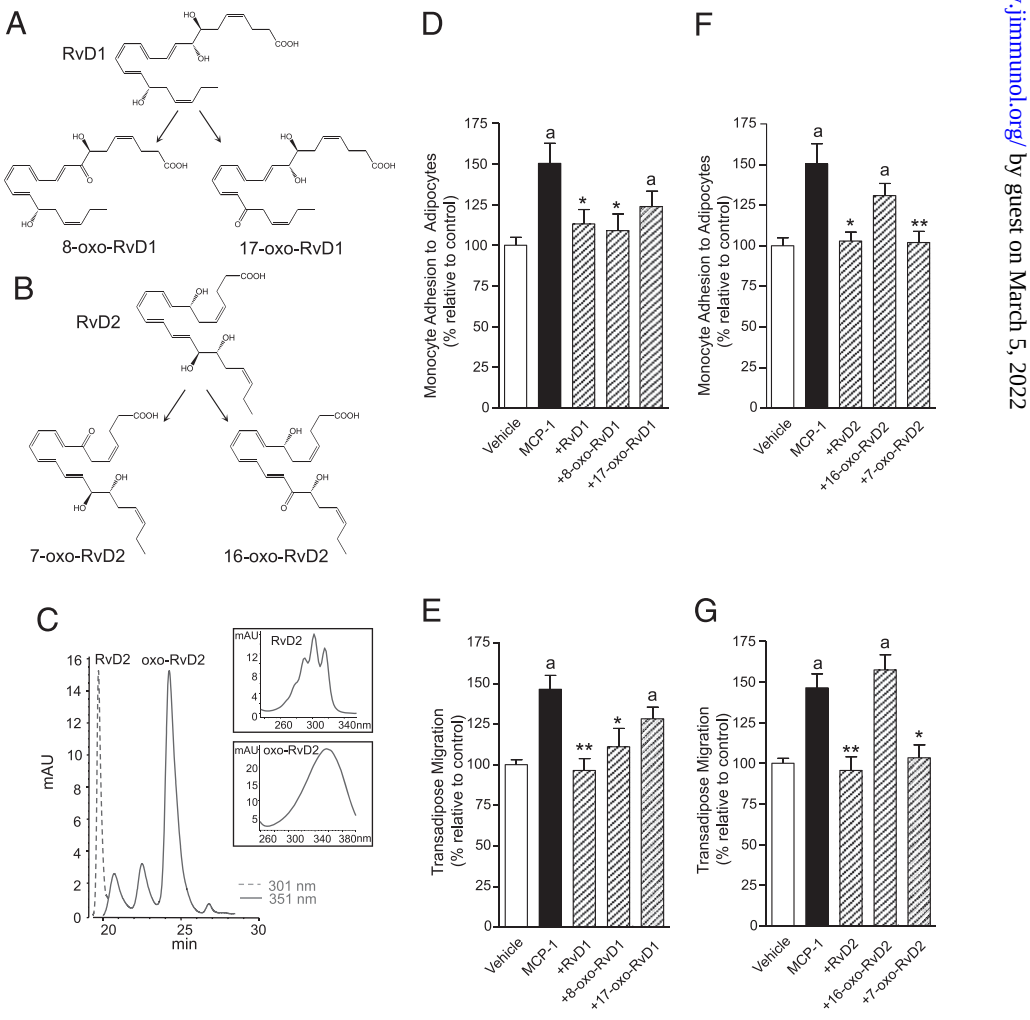

FIGURE 8. RvD2 conversion via 15-PGDH and actions of novel Rv metabolites on monocyte–adipocyte interactions. (**A**) The initial step in RvD1 conversion is dehydrogenation to yield 8-oxo-RvD1 or 17-oxo-RvD1. (**B**) Conversion of RvD2 by dehydrogenation to yield 7-oxo-RvD2 or 16-oxo-RvD2. (**C**) HPLC chromatogram of RvD2 (λ_{max}^{MeOH} = 301, dotted line) and novel oxo-RvD2 metabolites (λ_{max}^{MeOH} = 351, solid line) generated by the incubation of RvD2 (1.5 mg) with recombinant EOR (0.5 U, 0.1 M Tris-HCl, 1 mM NAD^+, pH 7.4) for 30 min at 37˚C. *Inset*, UV absorbance of RvD2 and the major oxo-containing peak eluting at 24.5 min. (**D**–**G**) Number of monocytes adhered to adipocytes and number of transmigrated monocytes in response to MCP-1 (15 ng/ml) in the presence of RvD1 metabolites (8-oxo-RvD1 and 17-oxo-RvD1) (D, E) and RvD2 metabolites (7-oxo-RvD2 and 16-oxo-RvD2) (F, G). The new RvD1- and RvD2-derived metabolites were produced using recombinant 15-PGDH, separated by RP-HPLC, extracted, and tested. Results are the mean ± SEM; n = 3 assayed in triplicate. *$p < 0.05$, **$p < 0.01$ versus cells exposed to MCP-1 alone; [a]$p < 0.05$ versus untreated vehicle.

inflammation in obese adipose tissue is the result of an inappropriate inflammatory response that remains uncontrolled.

A key finding of this study is that each of the resolution agonists RvD1 and RvD2 rescue the impaired phenotype of obese adipose tissue by enhancing expression and secretion of adiponectin in parallel with decreasing the secretion of proinflammatory adipokines/cytokines including leptin, TNF-α, IL-6, and IL-1β. Rvs also reduced monocyte–adipocyte adhesion, as well as monocyte transadipose migration, a likely key event in the return of inflamed adipose tissue to homeostasis. The actions of RvD1 and RvD2 were neither additive nor synergistic. Moreover, these results establish that an individual member of the Rv family, RvD2, is enzymatically further metabolized in adipose tissue via NAD^+-dependent dehydrogenation of the hydroxyl group at carbon 7 to form 7-oxo-RvD2. This novel 7-oxo-RvD2 metabolite retained the anti-inflammatory actions of RvD2 in reducing both monocyte adhesion and transmigration with adipocytes.

Of interest, results from several recent studies demonstrate that many metabolic functions are controlled by circadian rhythm proteins (29). Although the direct influence of circadian rhythms on SPM and endogenous mechanisms in the resolution of inflammation remains largely unexplored, the circadian release of glucocorticoids is known, and their link to downstream anti-inflammatory and proresolution mediator annexin A1 facilitates the return to homeostasis (30). Along these lines, PG 15d-PGJ_2, which can display anti-inflammatory properties, has recently been identified as an entrainment factor aligned with circadian oscillations (31). In light of these findings, it is plausible that local biosynthesis of SPM is controlled, in part, by circadian and stress responses (32) in various organs and tissues.

In line with the organ- and tissue-protective actions of SPM (8), proresolving mediators such as RvD1 and RvD1 skew adipose tissue macrophages toward a unique proresolving phenotype, ameliorating the incidence of obesity-related metabolic disorders (33, 34). Hence, enhancing local SPM production in adipose tissue, specifically those of the D-series Rvs and protectins, could reduce the inflammatory tone of obese adipose tissues. In turn, the local reduction of adipose inflammation by proresolving mediators such as RvD1 and RvD2 may reduce the adverse systemic impact of metabolic syndromes.

Acknowledgments

We thank M.H. Small for assistance with the manuscript.

Disclosures

C.N.S. is an inventor on patents (Rvs) assigned to Brigham and Women's Hospital and licensed to Resolvyx Pharmaceuticals. C.N.S. is a scientific founder of Resolvyx Pharmaceuticals and owns equity in the company. C.N.S.'s interests were reviewed and are managed by the Brigham and Women's Hospital and Partners HealthCare in accordance with their conflict of interest policies. The other authors have no financial conflicts of interest.

References

1. Ferrante, A. W., Jr. 2007. Obesity-induced inflammation: a metabolic dialogue in the language of inflammation. *J. Intern. Med.* 262: 408–414.
2. Ouchi, N., J. L. Parker, J. J. Lugus, and K. Walsh. 2011. Adipokines in inflammation and metabolic disease. *Nat. Rev. Immunol.* 11: 85–97.
3. Hotamisligil, G. S. 2006. Inflammation and metabolic disorders. *Nature* 444: 860–867.
4. Lumeng, C. N., and A. R. Saltiel. 2011. Inflammatory links between obesity and metabolic disease. *J. Clin. Invest.* 121: 2111–2117.
5. Zeyda, M., and T. M. Stulnig. 2007. Adipose tissue macrophages. *Immunol. Lett.* 112: 61–67.
6. Weisberg, S. P., D. McCann, M. Desai, M. Rosenbaum, R. L. Leibel, and A. W. Ferrante, Jr. 2003. Obesity is associated with macrophage accumulation in adipose tissue. *J. Clin. Invest.* 112: 1796–1808.
7. Serhan, C. N., S. D. Brain, C. D. Buckley, D. W. Gilroy, C. Haslett, L. A. J. O'Neill, M. Perretti, A. G. Rossi, and J. L. Wallace. 2007. Resolution of inflammation: state of the art, definitions and terms. *FASEB J.* 21: 325–332.
8. Serhan, C. N. 2007. Resolution phase of inflammation: novel endogenous anti-inflammatory and proresolving lipid mediators and pathways. *Annu. Rev. Immunol.* 25: 101–137.
9. González-Périz, A., R. Horrillo, N. Ferré, K. Gronert, B. Dong, E. Morán-Salvador, E. Titos, M. Martínez-Clemente, M. López-Parra, V. Arroyo, and J. Clària. 2009. Obesity-induced insulin resistance and hepatic steatosis are alleviated by omega-3 fatty acids: a role for resolvins and protectins. *FASEB J.* 23: 1946–1957.
10. Todoric, J., M. Löffler, J. Huber, M. Bilban, M. Reimers, A. Kadl, M. Zeyda, W. Waldhäusl, and T. M. Stulnig. 2006. Adipose tissue inflammation induced by high-fat diet in obese diabetic mice is prevented by n-3 polyunsaturated fatty acids. *Diabetologia* 49: 2109–2119.
11. Ramel, A., A. Martinéz, M. Kiely, G. Morais, N. M. Bandarra, and I. Thorsdottir. 2008. Beneficial effects of long-chain n-3 fatty acids included in an energy-restricted diet on insulin resistance in overweight and obese European young adults. *Diabetologia* 51: 1261–1268.
12. Petro, A. E., J. Cotter, D. A. Cooper, J. C. Peters, S. J. Surwit, and R. S. Surwit. 2004. Fat, carbohydrate, and calories in the development of diabetes and obesity in the C57BL/6J mouse. *Metabolism* 53: 454–457.
13. Yang, R., N. Chiang, S. F. Oh, and C. N. Serhan. 2011. Metabolomics-lipidomics of eicosanoids and docosanoids generated by phagocytes. *Curr. Protoc. Immunol.* 95:14.26.11–14.26.26.
14. Kasuga, K., R. Yang, T. F. Porter, N. Agrawal, N. A. Petasis, D. Irimia, M. Toner, and C. N. Serhan. 2008. Rapid appearance of resolvin precursors in inflammatory exudates: novel mechanisms in resolution. *J. Immunol.* 181: 8677–8687.
15. Serhan, C. N., R. Yang, K. Martinod, K. Kasuga, P. S. Pillai, T. F. Porter, S. F. Oh, and M. Spite. 2009. Maresins: novel macrophage mediators with potent antiinflammatory and proresolving actions. *J. Exp. Med.* 206: 15–23.
16. Krishnamoorthy, S., A. Recchiuti, N. Chiang, S. Yacoubian, C.-H. Lee, R. Yang, N. A. Petasis, and C. N. Serhan. 2010. Resolvin D1 binds human phagocytes with evidence for proresolving receptors. *Proc. Natl. Acad. Sci. USA* 107: 1660–1665.
17. Shimizu, T. 2009. Lipid mediators in health and disease: enzymes and receptors as therapeutic targets for the regulation of immunity and inflammation. *Annu. Rev. Pharmacol. Toxicol.* 49: 123–150.
18. Quinn, C. E., P. K. Hamilton, C. J. Lockhart, and G. E. McVeigh. 2008. Thiazolidinediones: effects on insulin resistance and the cardiovascular system. *Br. J. Pharmacol.* 153: 636–645.
19. Bazzoni, F., N. Tamassia, M. Rossato, and M. A. Cassatella. 2010. Understanding the molecular mechanisms of the multifaceted IL-10-mediated anti-inflammatory response: lessons from neutrophils. *Eur. J. Immunol.* 40: 2360–2368.
20. Sun, Y.-P., S. F. Oh, J. Uddin, R. Yang, K. Gotlinger, E. Campbell, S. P. Colgan, N. A. Petasis, and C. N. Serhan. 2007. Resolvin D1 and its aspirin-triggered 17R epimer. Stereochemical assignments, anti-inflammatory properties, and enzymatic inactivation. *J. Biol. Chem.* 282: 9323–9334.
21. Clish, C. B., Y. P. Sun, and C. N. Serhan. 2001. Identification of dual cyclooxygenase-eicosanoid oxidoreductase inhibitors: NSAIDs that inhibit PG-LX reductase/LTB(4) dehydrogenase. *Biochem. Biophys. Res. Commun.* 288: 868–874.
22. Tomlinson, J. W., and P. M. Stewart. 2002. The functional consequences of 11beta-hydroxysteroid dehydrogenase expression in adipose tissue. *Horm. Metab. Res.* 34: 746–751.
23. Brozic, P., B. Golob, N. Gomboc, T. L. Rizner, and S. Gobec. 2006. Cinnamic acids as new inhibitors of 17beta-hydroxysteroid dehydrogenase type 5 (AKR1C3). *Mol. Cell. Endocrinol.* 248: 233–235.
24. Tai, H. H., C. M. Ensor, M. Tong, H. Zhou, and F. Yan. 2002. Prostaglandin catabolizing enzymes. *Prostaglandins Other Lipid Mediat.* 68–69: 483–493.
25. Eltzschig, H. K., and P. Carmeliet. 2011. Hypoxia and inflammation. *N. Engl. J. Med.* 364: 656–665.
26. Ye, J. 2009. Emerging role of adipose tissue hypoxia in obesity and insulin resistance. *Int. J. Obes. (Lond.)* 33: 54–66.
27. Serhan, C. N. 2004. A search for endogenous mechanisms of anti-inflammation uncovers novel chemical mediators: missing links to resolution. *Histochem. Cell Biol.* 122: 305–321.
28. White, P. J., M. Arita, R. Taguchi, J. X. Kang, and A. Marette. 2010. Transgenic restoration of long-chain n-3 fatty acids in insulin target tissues improves resolution capacity and alleviates obesity-linked inflammation and insulin resistance in high-fat-fed mice. *Diabetes* 59: 3066–3073.
29. Eckle, T., K. Hartmann, S. Bonney, S. Reithel, M. Mittelbronn, L. A. Walker, B. D. Lowes, J. Han, C. H. Borchers, P. M. Buttrick, et al. 2012. Adora2b-elicited Per2 stabilization promotes a HIF-dependent metabolic switch crucial for myocardial adaptation to ischemia. *Nat. Med.* 18: 774–782.
30. Perretti, M., and F. D'Acquisto. 2009. Annexin A1 and glucocorticoids as effectors of the resolution of inflammation. *Nat. Rev. Immunol.* 9: 62–70.
31. Nakahata, Y., M. Akashi, D. Trcka, A. Yasuda, and T. Takumi. 2006. The in vitro real-time oscillation monitoring system identifies potential entrainment factors for circadian clocks. *BMC Mol. Biol.* 7: 5.
32. Csermely P., T. Korcsmáros, and K. Sulyok, eds. 2007. *Stress Responses in Biology and Medicine: Stress of Life in Molecules, Cells, Organisms, and Psychosocial Communities.* Blackwell Publishing, Boston.
33. Titos, E., B. Rius, A. González-Périz, C. López-Vicario, E. Morán-Salvador, M. Martínez-Clemente, V. Arroyo, and J. Clària. 2011. Resolvin D1 and its precursor docosahexaenoic acid promote resolution of adipose tissue inflammation by eliciting macrophage polarization toward an M2-like phenotype. *J. Immunol.* 187: 5408–5418.
34. Hellmann, J., Y. Tang, M. Kosuri, A. Bhatnagar, and M. Spite. 2011. Resolvin D1 decreases adipose tissue macrophage accumulation and improves insulin sensitivity in obese-diabetic mice. *FASEB J.* 25: 2399–2407.